

Defect Detection by MIMO Wireless Sensing based on Weighted Low-Rank plus Sparse Recovery

Udaya S.K.P. Miriya Thantrige^{*} Ali Kariminezhad[†] Peter Jung[‡] Aydin Sezgin^{*}

^{*} Ruhr-University Bochum, Bochum, Germany.

[†] Department of Autonomous Driving, Elektronische Fahrwerksysteme GmbH, Gaimersheim, Germany.

[‡] Institute of Communications and Information Theory, Technical University Berlin, Berlin, Germany.

{udaya.miriyathantrige, aydin.sezgin}@rub.de, ali.kariminezhad@efs-auto.com, peter.jung@tu-berlin.de.

Abstract—We address the detection of material defects, which are inside a layered material structure by multiple input multiple output (MIMO) wireless sensing from compressive measurements. However, due to reflections from the surface of the layered material structure the defect detection is challenging. To cope with this challenge, advanced signal processing methods are required. By utilizing a low-rank nature of the reflections of the layered material structure and sparse nature of the defects, we propose a method based on rank minimization and sparse recovery. To obtain a higher accuracy in the recovery of low-rank and sparse components, we propose a non-convex approach based on the iteratively reweighted nuclear norm and iteratively reweighted ℓ_1 -norm algorithm. Our numerical results show that the proposed method is able to demix and recover the signalling responses of the defects and layered structure successfully from substantially reduced number of observations. Further, the proposed approach outperforms the state-of-the-art clutter reduction approaches.

Index Terms—Low-rank, sparse recovery, signal separation, compressed sensing.

I. INTRODUCTION

Non-destructive testing (NDT) and characterization of material is of high relevance for many industrial sectors. Further, the NDT characterization of material using electromagnetic (EM) waves has several potential applications such as defect detection [1], through the wall (TWR) object identification [2], material characterization [3] and multi-layer target detection [4]. The main challenge of the detection of defects/objects is the strong clutter due to the reflection from the surface of the layered material structure [5], [6]. The conventional clutter suppression methods such as background subtraction (BS), spatial filtering (SF) [2], and subspace projection (SP) [7] are not effective in suppressing this kind of clutter. This is due to the fact that the BS requires reference data of the scene, which is not available most of the time. Also, in the SP, it is difficult to determine the perfect threshold for clutter removal.

Many compressed sensing (CS)-based methods were proposed

for object identification from very few measurements [8]–[13]. Moreover, joint clutter reduction and object recovery have been introduced recently in CS by considering that the clutter resides in a low-rank subspace while the response of the objects is sparse [9]–[11]. However, finding matrices of lowest rank and sparsest vectors from compressed observations are usually NP-hard problems. Thus, it is common to consider convex relaxations to rank and sparsity in terms of the nuclear norm [14], [15] of a matrix (sum of singular values) and the ℓ_1 -norm of a vector (absolute sum of elements). In both cases non-convex approaches are known to perform better by providing tighter characterizations of rank and sparsity. In the ℓ_1 -minimization algorithms, larger coefficients are heavily penalized compared to the smaller coefficients and iteratively reweighted ℓ_1 -minimization has been considered in this context [16], [17]. Similarly, nuclear norm minimization algorithms shrink singular values equally and tighter approaches based on reweighting has been considered here as well [18]–[21].

In this work, we propose a novel iterative alternating direction method of multipliers (ADMM)-based algorithm for defect detection from few compressive measurements which combines iteratively reweighted nuclear norm and ℓ_1 -minimization. We compare the performance of our method with state-of-the-art clutter-reduction methods such as SF, SP and the low-rank plus sparse recovery method presented in [9]. The paper is organized as follows. We introduce the system model in Section II and present the recovery algorithm in Section III. In Section IV, we evaluate our approach numerically.

II. SYSTEM MODEL

Consider a mono-static stepped-frequency continuous (SFCW) radar with M transceivers as shown in Fig. 1. The transceivers are placed parallel to the single-layered material structure while maintaining an equal distance between transceivers. Here, we consider P static defects, which are inside the layered material structure. Each transceiver transmits a stepped-frequency signal containing N frequencies which

This work was funded by the Deutsche Forschungsgemeinschaft (DFG, German Research Foundation) – Project-ID 287022738 – TRR 196 (S02 project). The two first authors have equal contributions.

are equally spaced over the bandwidth of B Hz. The received signal of the m -th antenna corresponding to n -th frequency band (f_n), $y_{m,n}$, consists of two components, namely, the reflection of the layered material structure, i.e., $y_{m,n}^l$ and the reflection of the defects, i.e., $y_{m,n}^d$. Considering transmission from the antennas in non-overlapping time periods, $y_{m,n}$ is given by $y_{m,n} = y_{m,n}^l + y_{m,n}^d + z_{m,n}$. Here, $z_{m,n}$ is the additive Gaussian noise. Now, $y_{m,n}^l \in \mathbb{C}$ in base-band is given by

$$y_{m,n}^l = \sum_{r=1}^{D+1} \alpha_r e^{-j2\pi f_n \tau_{m,r}}. \quad (1)$$

Here, $\alpha_r \in \mathbb{C}$ and $\tau_{m,r} \in \mathbb{R}$ are the complex signal strength and the propagation delay of the r -th return of the layered structure. The number of internal reflections within the layered structure is given by D . Now, the received signal of the layered structure for all N frequencies is given by $\mathbf{y}_m^l = [y_{m,1}^l, \dots, y_{m,N}^l]^T \in \mathbb{C}^N$. The reflection of the defects, $y_{m,n}^d \in \mathbb{C}$ in base-band is given by

$$y_{m,n}^d = \sum_{p=1}^P \alpha_p e^{-j2\pi f_n \tau_{m,p}}. \quad (2)$$

Here, $\alpha_p \in \mathbb{C}$ is the complex signal strength of the p -th defect and $\tau_{m,p}$ is the round-travel time of the signal from the m -th antenna location to the p -th defect and back. To this end, the received signal of the defects for all N frequencies by the m -th antenna is given by $\mathbf{y}_m^d = [y_{m,1}^d, \dots, y_{m,N}^d]^T \in \mathbb{C}^N$.

Next, the scene is considered to be hypothetically partitioned into a rectangular grid of size Q as shown in Fig. 1 to form a two-dimensional image of the scene. Now, a vector $\mathbf{s} \in \mathbb{C}^{Q \times 1}$ contains all the α_p values of the defects. Then, \mathbf{y}_m^d can be written as

$$\mathbf{y}_m^d = \mathbf{A}_m \mathbf{s}. \quad (3)$$

The (n, q) -th element of the matrix $\mathbf{A}_m \in \mathbb{C}^{N \times Q}$ is given by $\exp(-j2\pi f_n \tau_{m,q})$. The propagation time delay between m -th antenna to the q -th grid location is given by $\tau_{m,q}$. Now, the received signal corresponding to all M antennas and N frequencies $\mathbf{Y} \in \mathbb{C}^{M \times N}$ is given by $\mathbf{Y} = \mathbf{Y}^l + \mathbf{Y}^d + \mathbf{Z}$. Here, \mathbf{Y}^l , \mathbf{Y}^d and $\mathbf{Z} \in \mathbb{C}^{M \times N}$ are the received signals of the layered structure, defects and noise, respectively. Let $\text{vec}(\cdot)$ denote the vectorization operator, which converts a matrix to a vector by stacking the columns of the matrix. To this end, $\text{vec}(\mathbf{Y}^l)$ and $\text{vec}(\mathbf{Y}^d)$ are given by $[(\mathbf{y}_1^l)^T, \dots, (\mathbf{y}_M^l)^T]^T$ and $[(\mathbf{y}_1^d)^T, \dots, (\mathbf{y}_M^d)^T]^T$, respectively. Further, $\text{vec}(\mathbf{Y}^d) = \mathbf{A} \mathbf{s}$, with $\mathbf{A} = [(\mathbf{A}_1)^T, \dots, (\mathbf{A}_M)^T]^T \in \mathbb{C}^{MN \times Q}$.

A. Compressed sensing (CS) approach

The CS approach considers that only a subset of antennas and frequencies are available. To this end, the reduced data vector $\mathbf{y}_{cs} \in \mathbb{C}^{K \times 1}$ of size K ($\ll MN$) is given by

$$\mathbf{y}_{cs} = \Phi (\text{vec}(\mathbf{Y})) = \Phi (\text{vec}(\mathbf{Y}^l) + \mathbf{A} \mathbf{s} + \text{vec}(\mathbf{Z})). \quad (4)$$

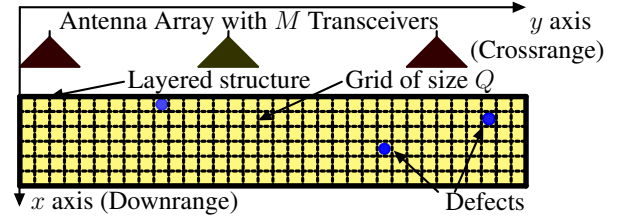


Fig. 1. Getting the measurements of a single-layered material structure using a radar with M transceivers.

Here, $\Phi \in \mathbb{R}^{K \times MN}$ is the selection matrix which has a single non-zero element of value 1 in each row to indicate the selected frequency of a particular antenna if that antenna is selected. Our objective is to recover the \mathbf{Y}^l and the \mathbf{s} from the reduced data vector \mathbf{y}_{cs} .

III. LOW-RANK PLUS SPARSE RECOVERY

The response of the layered structure at different antennas shows strong similarity, i.e., \mathbf{Y}^l is low-rank. Moreover, the number of defects which are inside the layered material structure is less than grid size Q . Therefore, we consider that the vector \mathbf{s} in (3) is sparse (few non-zero entries). Thus, the estimation of \mathbf{Y}^l and \mathbf{s} from \mathbf{y}_{cs} is formulated as a low-rank plus sparse recovery problem. However, rank and sparsity minimization problems are usually NP-hard and therefore convex relaxations based on the nuclear norm and ℓ_1 -norm are considered. The resulting convex problems are meanwhile well understood on the theoretical level but are often empirically outperformed by several non-convex approaches. A well-known approach is based on iterative reweighting. To this end, the estimation of \mathbf{Y}^l and \mathbf{s} from \mathbf{y}_{cs} is formulated as

$$\begin{aligned} \min_{\mathbf{Y}^l, \mathbf{s}} \quad & \beta_L \|\mathbf{W}_1 \mathbf{Y}^l \mathbf{W}_2\|_* + \beta_S \|\mathbf{W}_s \mathbf{s}\|_1, \\ \text{s.t.} \quad & \|\mathbf{y}_{cs} - \Phi \text{vec}(\mathbf{Y}^l) - \Phi \mathbf{A} \mathbf{s}\|_2^2 \leq \epsilon. \end{aligned} \quad (5)$$

Here, β_L and β_S are given regularization parameters and ϵ is a small positive constant (noise bound). The ℓ_1 -norm of a vector and nuclear norm of a matrix are represented by $\|\cdot\|_1$ and $\|\cdot\|_*$, respectively. Further, $\mathbf{W}_1 \in \mathbb{C}^{M \times M}$, $\mathbf{W}_2 \in \mathbb{C}^{N \times N}$ are complex weight matrices and $\mathbf{W}_s \in \mathbb{R}^{Q \times Q}$ is a non-negative diagonal weight matrix. Due to its multi-objective nature, problem in eq. (5) is challenging and therefore the alternating direction method of multipliers (ADMM) is used [22]. Let the signal component at the t -th ADMM iteration be denoted as $(\cdot)^t$ and $\mathbf{u} \in \mathbb{C}^{K \times 1}$ and $\rho > 0$ are the auxiliary coupling variable and penalty factor related to the ADMM approach, respectively. Now, \mathbf{Y}^l at the $(t+1)$ -th iteration is the solution of the nuclear norm minimization for fixed weights, which can be formulated as a semi-definite program (SDP)

problem [20], [23]

$$\begin{aligned}
(\mathbf{Y}^l)^{t+1} &= \arg \min_{\mathbf{Y}^l, \mathbf{L}, \mathbf{R}} \frac{\beta_L}{2} (\text{Tr}((\mathbf{W}_1)^t \mathbf{L}) + \text{Tr}((\mathbf{W}_2)^t \mathbf{R})) + \\
&\quad \frac{\rho}{2} \left\| \Phi \text{vec}(\mathbf{Y}^l) + \Phi \mathbf{A}(\mathbf{s})^t - \mathbf{y}_{cs} + \frac{1}{\rho} (\mathbf{u})^t \right\|_2^2, \quad (6) \\
\text{s.t.} \quad &\begin{bmatrix} \mathbf{L} & \mathbf{Y}^l \\ (\mathbf{Y}^l)^H & \mathbf{R} \end{bmatrix} \succeq 0.
\end{aligned}$$

Notice that, the matrices $\mathbf{L} = \mathbf{L}^H \in \mathbb{C}^{M \times M}$ and $\mathbf{R} = \mathbf{R}^H \in \mathbb{C}^{N \times N}$ are auxiliary variables. The matrices $(\mathbf{W}_1)^t \in \mathbb{C}^{M \times M}$ and $(\mathbf{W}_2)^t \in \mathbb{C}^{N \times N}$ are weight matrices, which are prone to optimization as well. For given $(\mathbf{W}_1)^t$ and $(\mathbf{W}_2)^t$ at t -th iteration which are positive semi-definite ($\mathbf{W}_1, \mathbf{W}_2 \succeq 0$), this problem is a convex optimization problem. Therefore, to update \mathbf{W}_1 and \mathbf{W}_2 , the eigenvectors of the \mathbf{L} and \mathbf{R} in the previous iteration are used. Let the eigenvectors of \mathbf{L} and \mathbf{R} be $\hat{\boldsymbol{\lambda}}$ and $\tilde{\boldsymbol{\lambda}}$, respectively. Now, $\mathbf{L} = \mathbf{U} \text{diag}(\hat{\boldsymbol{\lambda}}^{(t)}) \mathbf{U}^H$ and $\mathbf{R} = \mathbf{V} \text{diag}(\tilde{\boldsymbol{\lambda}}^{(t)}) \mathbf{V}^H$. Next, to update \mathbf{W}_1 and \mathbf{W}_2 for the $(t+1)$ -th iteration a decay function $f(\cdot)$ is used

$$\boldsymbol{\gamma}_L^{(t)} = f(\hat{\boldsymbol{\lambda}}^{(t)}) \quad \text{and} \quad \boldsymbol{\gamma}_R^{(t)} = f(\tilde{\boldsymbol{\lambda}}^{(t)}) \quad (7)$$

$$\begin{aligned}
(\mathbf{W}_1)^{t+1} &= \mathbf{U} \text{diag}(\boldsymbol{\gamma}_L^{(t)}) \mathbf{U}^H, \\
(\mathbf{W}_2)^{t+1} &= \mathbf{V} \text{diag}(\boldsymbol{\gamma}_R^{(t)}) \mathbf{V}^H.
\end{aligned} \quad (8)$$

The operator $\text{diag}(\cdot)$ takes a vector as an input and returns a square diagonal matrix in which the main diagonal contains the vector elements and zeros elsewhere. In this paper, the log-determinant heuristic [20] is used as the decay function f . Now, $\boldsymbol{\gamma}_L^{(t)}$ and $\boldsymbol{\gamma}_R^{(t)}$ in (8) are given by

$$\boldsymbol{\gamma}_L^{(t)} = (\hat{\boldsymbol{\lambda}}^{(t)} + \delta \mathbf{1}_M)^{-1} \quad \text{and} \quad \boldsymbol{\gamma}_R^{(t)} = (\tilde{\boldsymbol{\lambda}}^{(t)} + \delta \mathbf{1}_N)^{-1}. \quad (9)$$

Here, δ is a positive constant and $\mathbf{1}_B$ represents a vector of length B with all elements equal to 1. Next, \mathbf{s} is updated as

$$\begin{aligned}
(\mathbf{s})^{t+1} &= \arg \min_{\mathbf{s}} \beta_S \left\| (\mathbf{W}_s)^t \mathbf{s} \right\|_1 + \\
&\quad \frac{\rho}{2} \left\| \Phi \text{vec}((\mathbf{Y}^l)^{t+1}) + \Phi \mathbf{A} \mathbf{s} - \mathbf{y}_{cs} + \frac{(\mathbf{u})^t}{\rho} \right\|_2^2. \quad (10)
\end{aligned}$$

The weight matrix for $t+1$ -th iteration $(\mathbf{W}_s)^{t+1}$ is given by

$$(\mathbf{W}_s)^{t+1} = \text{diag} \left((|(\mathbf{s})^{t+1}| + \delta \mathbf{1}_Q)^{-1} \right). \quad (11)$$

Finally, \mathbf{u} is updated as

$$(\mathbf{u})^{t+1} = (\mathbf{u})^t + \rho (\Phi \text{vec}((\mathbf{Y}^l)^{t+1}) + \Phi \mathbf{A}(\mathbf{s})^{t+1} - \mathbf{y}_{cs}). \quad (12)$$

The three main ADMM steps are given in eqs. (6), (10) and (12), which are performed iteratively as shown in Alg. 1 to estimate the \mathbf{Y}^l and \mathbf{s} . In this work, we propose two versions of Alg. 1 named as low-rank plus sparse recovery with single

Algorithm 1: Low-rank-plus-sparse recovery algorithm

Input: \mathbf{y}_{cs} , $\epsilon = 10^{-8}$, maximum number of outer and inner iterations (T and J), Φ , \mathbf{A} .
Initialization: $\rho = 10^{-2}$, $\rho_o = 1.05$, $\rho_m = 10^3$, $t = 0$, $(\mathbf{Y}^l)^0 = \text{vec}^{-1}(\Phi^\dagger \mathbf{y}_{cs})$, $(\mathbf{s})^0 = \mathbf{0}_Q$, $(\mathbf{W}_s)^1 = \text{diag}(\mathbf{1}_Q)$, $(\mathbf{u})^0 = \mathbf{0}_K$, $(\mathbf{W}_1)^1 = \text{diag}(\mathbf{1}_M)$, $(\mathbf{W}_2)^1 = \text{diag}(\mathbf{1}_N)$.
while $\|\Phi \text{vec}(\mathbf{Y}^l) + \Phi \mathbf{A} \mathbf{s} - \mathbf{y}_{cs}\|_2^2 > \epsilon$ **or** $t < T$ **do**
 ADMM step 1: Update \mathbf{Y}^l
 for $j \leftarrow 1$ **To** $J+1$ **By** 1 **do**
 if $j = 1$ **then** $(\mathbf{W}_1)^j = (\mathbf{W}_1)^t$, $(\mathbf{W}_2)^j = (\mathbf{W}_2)^t$.
 Update $(\mathbf{Y}^l)^{j+1}$ by eq. (6).
 Update $(\mathbf{W}_1)^{j+1}$ and $(\mathbf{W}_2)^{j+1}$ by eq. (8) and (9).
 $(\mathbf{Y}^l)^{t+1} = (\mathbf{Y}^l)^{j+1}$, $(\mathbf{W}_1)^{t+1} = (\mathbf{W}_1)^{j+1}$ and $(\mathbf{W}_2)^{t+1} = (\mathbf{W}_2)^{j+1}$.
 ADMM step 2: Update \mathbf{s}
 for $j \leftarrow 1$ **To** $J+1$ **By** 1 **do**
 if $j = 1$ **then** $(\mathbf{W}_s)^j = (\mathbf{W}_s)^t$.
 Update $(\mathbf{s})^{j+1}$ by eq. (10).
 Update $(\mathbf{W}_s)^{j+1}$ by eq. (11).
 $(\mathbf{s})^{t+1} = (\mathbf{s})^{j+1}$ and $(\mathbf{W}_s)^{t+1} = (\mathbf{W}_s)^{j+1}$.
 ADMM step 3: Update \mathbf{u} , ρ and t
 Update $(\mathbf{u})^{t+1}$ by eq. (12).
 $\rho = \min(\rho_o \times \rho, \rho_m)$, and $t = t + 1$.
Output: \mathbf{Y}^l , \mathbf{s} .

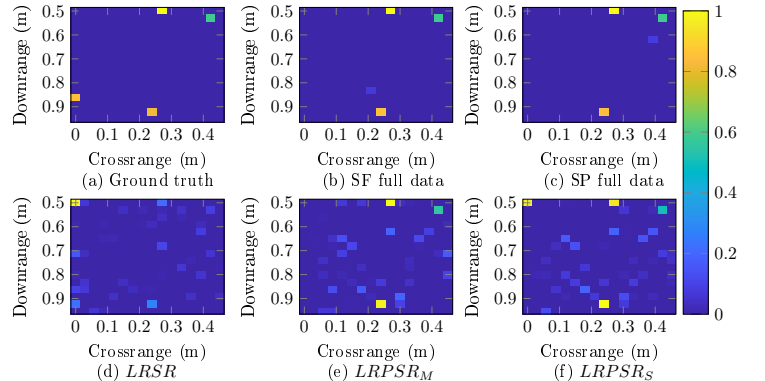


Fig. 2. Image of the defects for SNR 20 dB: (a) Ground truth. (b), (c) SF and SP with 100% of data, (d), (e), (f) LRSR [9], LRPSR_M and LRPSR_S with 30% of data ($K/MN = 30\%$).

inner ADMM loop (LRPSR_S) and low-rank plus sparse recovery with multiple inner ADMM loops (LRPSR_M), respectively. In the LRPSR_S, a single inner loop in the ADMM steps 1 and 2 is used (i.e., $J = 0$ in Alg. 1), while in the LRPSR_M J is set to 5. Further, $\text{vec}^{-1}(\cdot)$ and $(\cdot)^\dagger$ represent vector to matrix conversion and pseudo inverse, respectively. Notice that, in Alg. 1, β_L , β_S and δ are set to 1, $1/\sqrt{\max(M, N)}$ and 1, respectively.

IV. SIMULATION RESULTS

First, a generic model was used to evaluate the performance of Alg. 1 generally. Next, simulations were performed based

on the SFCW radar model given in Section II.

A. Tests with generic Gaussian model

Here, the number of non-zero elements of the ground truth sparse vector \mathbf{s}_T is set as $N_d = 4$ and the rank of the ground truth low-rank matrix \mathbf{Y}_T^l is set to 2. The elements of \mathbf{A} are generated as i.i.d. $\mathcal{N}(0, 1)$. \mathbf{y}_{cs} is given by (4) where the non-zero positions of Φ are selected uniformly at random. The signal-to-noise ratio is $\text{SNR} := \|\text{vec}(\mathbf{Y}_T^l) + \mathbf{A}\mathbf{s}_T\|_2^2 / \|\mathbf{Z}\|_F^2 = 20\text{dB}$ and $M = 10$, $N = 20$ and $Q = 256$.

To quantify the recovery of defects, we use the target-to-clutter ratio $\text{TCR} := \frac{Q - N_d}{N_d} \sum_{q \in A_d} |s[q]|^2 / \sum_{q \notin A_d} |s[q]|^2$, where $A_d = \{i | s_T[i] \neq 0\}$ contains the actual locations of the N_d defects. The average $\text{TCR}[\text{dB}]$ for 100 simulations is:

Compression ratio (K/MN)	SP	SF	LRSR	LRPSR _M	LRPSR _S
30%	19.62	47.00	21.44	26.43	21.77
40%			21.85	31.29	26.26
50%			22.07	33.00	32.92

Here, the full data set (i.e., compression ratio (K/MN) = 100%) is utilized for the spatial filtering (SF) and subspace projection (SP) and only for these methods it is assumed that N_d is known. As such, SF only serves as a benchmark. It can be observed that both the proposed approaches, LRPSR_M and LRPSR_S, outperform SP and the method presented in [9] (LRSR). Moreover, LRPSR_M improves over LRPSR_S.

B. Tests with SFCW radar model

Simulations were performed based on the SFCW radar model with a carrier frequency f_c of 300 GHz, bandwidth B as 5 GHz, N as 20 and M as 10. The inter-antenna spacing is chosen as half of the wavelength of f_c . Here, a single-layered structure with both height and length of 0.5 m is used. The distance from the antenna array to the front surface of the layered structure is 0.5 m. The scene is partitioned into a 16×16 grid with equal grid size. The grid size is chosen according to the Rayleigh resolution of the radar. The signal strength of the layered structure α_r is considered 10 times stronger than the maximum signal strength of the defects α_p . In the simulations, four defects are considered.

The images formed using different clutter-reduction methods are shown in Fig. 2. Here, to obtain an image of the defects, the recovered vector \mathbf{s} is reshaped into a matrix. Fig. 2(a) shows the actual defect locations. Fig. 2(b) and 2(c) show the results of the SF and SP for the full data set. Fig. 2(d), 2(e) and 2(f) show the result of the LRSR [9] and the proposed approaches LRPSR_M and LRPSR_S. It can be seen that the proposed LRPSR_M and LRPSR_S approaches are able to identify three out of four defects using only 30% of the data. Further, it is observed that defect detection with LRPSR_M and LRPSR_S perform similar to the state-of-the-art SP and SF even with reduced data set. The TCR values of Fig. 2 for the SF, SP, LRSR, LRPSR_M and LRPSR_S are 71.4 dB, 70.2 dB, 30.8 dB, 52.3 dB, and 44.3 dB, respectively. Higher TCR value means higher clutter reduction and the results show that the proposed approaches achieved satisfactory TCR values.

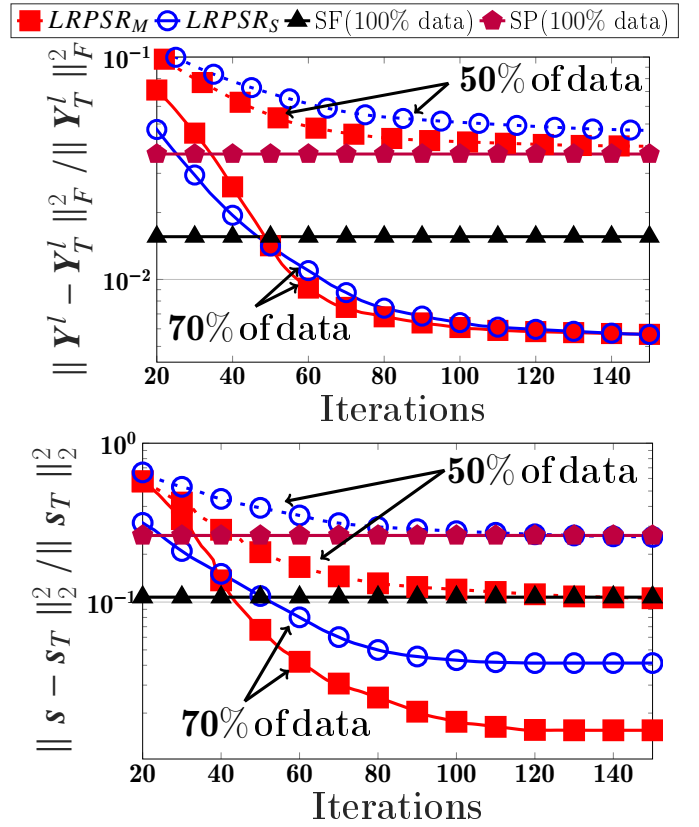


Fig. 3. Average recovery error of low-rank (top) and sparsity (bottom) contributions.

Fig. 3 shows the average mean square error (MSE) of the recovered low-rank and sparse components with respect to the iterations (t) of Alg. 1 for 20 simulations. Here, SNR, M and N are set to 30 dB, 10, and 10, respectively. The MSE of the recovered low-rank and sparse components for a single simulation are given as $\|\mathbf{Y}^l - \mathbf{Y}_T^l\|_F^2 / \|\mathbf{Y}_T^l\|_F^2$ and $\|\mathbf{s} - \mathbf{s}_T\|_2^2 / \|\mathbf{s}_T\|_2^2$, respectively. Based on Fig. 3, it can be observed that the LRPSR_M outperforms LRPSR_S. Further, it can be observed that as the compression ratio decreases, the improvement of LRPSR_M compared to the LRPSR_S increases. Moreover, the proposed LRPSR_M and LRPSR_S outperform state-of-the-art SP and SF in low-rank and sparse recovery with only 70% of data.

V. CONCLUSION

In this work, the low-rank plus sparse recovery approach is proposed for defect detection in the presence of strong clutter of the layered material structure. To this end, an iterative algorithm is developed based on ADMM for defect detection with iterative reweighted NN and ℓ_1 -norm minimization. Moreover, multiple inner loops in the ADMM low-rank and sparse update steps improve the low-rank and sparse recovery. The results show that the proposed approaches are able to improve defect detection with reduced data set.

REFERENCES

- [1] C.D. Stoik, M.J. Bohn, and J.L. Blackshire, "Nondestructive evaluation of aircraft composites using transmissive Terahertz time domain spectroscopy," *Optics express*, vol. 16, no. 21, pp. 17039–17051, 2008.
- [2] Y. S. Yoon and M. G. Amin, "Spatial filtering for wall-clutter mitigation in through-the-wall radar imaging," *IEEE Trans. on Geosci. and Remote Sens.*, vol. 47, no. 9, pp. 3192–3208, 2009.
- [3] U. S. K. P. M. Thanthrige, J. Barowski, I. Rolfes, D. Erni, T. Kaiser, and A. Sezgin, "Characterization of dielectric materials by sparse signal processing with iterative dictionary updates," *IEEE Sens. Lett.*, vol. 4, no. 9, pp. 1–4, 2020.
- [4] A. Kariminezhad and A. Sezgin, "Spatio-temporal waveform design in active sensing systems with multilayer targets," *2019 27th EUSIPCO*, pp. 1–5, 2019.
- [5] F. H. C. Tivive, A. Bouzerdoum, and M. G. Amin, "An SVD-based approach for mitigating wall reflections in through-the-wall radar imaging," *2011 IEEE Radar Conf.*, pp. 519–524, 2011.
- [6] F. H. C. Tivive, A. Bouzerdoum, and M. G. Amin, "A subspace projection approach for wall clutter mitigation in through-the-wall radar imaging," *IEEE Trans. on Geosci. and Remote Sens.*, vol. 53, no. 4, pp. 2108–2122, 2014.
- [7] U. S. Khan and W. Al-Nuaimy, "Background removal from GPR data using eigenvalues," *Proc. of the XIII Int. Conf. on Ground Penetrating Radar*, pp. 1–5, 2010.
- [8] V. H. Tang, A. Bouzerdoum, S. L. Phung, and F. H. C. Tivive, "Enhanced wall clutter mitigation for compressed through-the-wall radar imaging using joint bayesian sparse signal recovery," *2014 IEEE ICASSP*, pp. 7804–7808, 2014.
- [9] V. H. Tang, A. Bouzerdoum, S. L. Phung, and F. H. C. Tivive, "Indoor scene reconstruction for through-the-wall radar imaging using low-rank and sparsity constraints," *2016 IEEE Radar Conf.*, pp. 1–4, 2016.
- [10] A. Bouzerdoum, V. H. Tang, and S. L. Phung, "A low-rank and jointly-sparse approach for multipolarization through-wall radar imaging," *2017 IEEE Radar Conf.*, pp. 0263–0268, 2017.
- [11] V. H. Tang, A. Bouzerdoum, S. L. Phung, and F. H. C. Tivive, "Radar imaging of stationary indoor targets using joint low-rank and sparsity constraints," *2016 IEEE ICASSP*, pp. 1412–1416, 2016.
- [12] Q. Huang, L. Qu, B. Wu, and G. Fang, "UWB through-wall imaging based on compressive sensing," *IEEE Trans. on Geosci. and Remote Sensing*, vol. 48, no. 3, pp. 1408–1415, 2009.
- [13] Y. S. Yoon and M. G. Amin, "Through-the-wall radar imaging using compressive sensing along temporal frequency domain," *2010 IEEE ICASSP*, pp. 2806–2809, 2010.
- [14] B. Recht, M. Fazel, and P. A. Parrilo, "Guaranteed Minimum-Rank Solutions of Linear Matrix Equations via Nuclear Norm Minimization," *SIAM Review*, vol. 52, no. 3, pp. 471–501, 2010.
- [15] C. Lu, J. Tang, S. Yan, and Z. Lin, "Nonconvex Nonsmooth Low Rank Minimization via Iteratively Reweighted Nuclear Norm," *IEEE Trans. on Image Proces.*, vol. 25, no. 2, pp. 829–839, 2016.
- [16] E. J. Candes, M. B. Wakin, and S. P. Boyd, "Enhancing sparsity by reweighted ℓ_1 minimization," *Journal of Fourier analysis and applications*, vol. 14, no. 5-6, pp. 877–905, 2008.
- [17] D. Wipf and S. Nagarajan, "Iterative reweighted ℓ_1 and ℓ_2 methods for finding sparse solutions," *IEEE J. Sel. Topics Signal Process.*, vol. 4, no. 2, pp. 317–329, 2010.
- [18] S. Gu, Q. Xie, D. Meng, W. Zuo, X. Feng, and L. Zhang, "Weighted nuclear norm minimization and its applications to low level vision," *Int. journal of computer vision*, vol. 121, no. 2, pp. 183–208, 2017.
- [19] M. Malek-Mohammadi, M. Babaie-Zadeh, and M. Skoglund, "Iterative concave rank approximation for recovering low-rank matrices," *IEEE Trans. on Signal Proces.*, vol. 62, no. 20, pp. 5213–5226, 2014.
- [20] M. Fazel, H. Hindi, and S. P. Boyd, "Log-det heuristic for matrix rank minimization with applications to Hankel and Euclidean distance matrices," *Proc. of the 2003 American Control Conf., 2003.*, vol. 3, pp. 2156–2162 vol.3, 2003.
- [21] C. Lu, J. Tang, S. Yan, and Z. Lin, "Nonconvex nonsmooth low rank minimization via iteratively reweighted Nuclear norm," *IEEE Trans. Image Process.*, vol. 25, no. 2, pp. 829–839, 2016.
- [22] C. Lu, J. Feng, S. Yan, and Z. Lin, "A unified alternating direction method of multipliers by majorization minimization," *IEEE Trans. Pattern Anal. Mach. Intell.*, vol. 40, no. 3, pp. 527–541, 2018.
- [23] M. Fazel, H. Hindi, S. P. Boyd, et al., "A rank minimization heuristic with application to minimum order system approximation," *Proc. of the American control conf.*, vol. 6, pp. 4734–4739, 2001.